PHYSICAL REVIEW B
CONDENSED MATTER

THIRD SERIES, VOLUME 51, NUMBER 9 1 MARCH 1995-I

First-principles temperature-pressure phase diagram of magnesium

John A. Moriarty
Lawrence Livermore National Laboratory, University of California, Livermore, California 94551

J. D. Althoff
Sandia National Laboratories, Livermore, California 94551
(Received 22 August 1994)

Using first-principles interatomic potentials derived from generalized pseudopotential theory, high-temperature solid-phase stability and melting in magnesium have been studied through a combination of analytic statistical methods and molecular-dynamics simulation. Extending our previous work on the hcp-bcc phase line in the solid below 1000 K [Phys. Rev. B **48**, 13 253 (1993)], a complete and accurate temperature-pressure phase diagram to 3500 K and 60 GPa has thereby been obtained. The rapidly temperature-dependent hcp-bcc phase line in the solid is predicted to end in a triple point on the melting curve near 1200 K and 4 GPa. Calculated melting properties at ambient pressure and the hcp-liquid melt line to 4 GPa are in good agreement with existing experimental data. The high-pressure, high-temperature hcp-bcc and bcc-liquid phase lines should be readily accessible to experimental investigation via the laser-heated diamond-anvil cell.

I. INTRODUCTION

The calculation of temperature-pressure phase diagrams in elemental materials from basic quantum-mechanical principles has been of long-standing interest in condensed-matter theory. Central to this task for any given material is the need for both an accurate and flexible total-energy functional, $E_{\rm tot}(\mathbf{R}_1 \cdots \mathbf{R}_N)$, which can express the configuration dependence of the energy for an arbitrary arrangement of the atoms. Modern density-functional quantum mechanics in the local-density approximation[1] (LDA) has provided a practical first-principles framework from which to proceed. At zero temperature, self-consistent LDA electronic-band-structure calculations of $E_{\rm tot}$ can explain both the observed structural trends at ambient pressure as well as pressure-induced solid-solid phase transitions.[2] In some cases it has even been possible to accurately predict high-pressure phase transitions prior to experiment, such as the hcp $\rightarrow$ bcc transition near 50 GPa in magnesium.[3,4] More difficult, however, is the temperature axis of the phase diagram where the high symmetry of the zero-temperature environment is lost. One effective strategy in this regard has been to develop $E_{\rm tot}$ systematically in terms of transferable interatomic potentials which apply equally to all phases of a material, both ordered and disordered, including the liquid. Within the framework of LDA quantum mechanics, this has been done successfully for simple and transition metals alike via generalized pseudopotential theory[3,5,6] (GPT) by expanding $E_{\rm tot}$ in terms of weak pseudopotential and d-state matrix elements coupling different sites. These interatomic potentials can then not only deal with the zero-temperature energetics and pressure-induced phase transitions, but they can be used together with appropriate statistical mechanics tools to treat temperature-induced solid-solid transitions and melting as well. In the case of magnesium, first-principles GPT potentials can accurately predict the hcp $\rightarrow$ bcc phase transition at zero temperature.[3,6] At the same time, these potentials yield an excellent description of ground-state cohesive properties, phonons, and thermodynamic properties, as was demonstrated in a recent study[6] of the temperature dependence of the hcp-bcc phase line to 1000 K. The purpose of this paper is to extend the application of these potentials to the high-temperature hcp, bcc, and liquid phases above 1000 K and thereby obtain the entire temperature-pressure phase diagram of magnesium below 3500 K and 60 GPa.

In addition to being a prototype case for theory, the phase diagram of magnesium is of special interest from a physical standpoint as well. Magnesium is the only element on the left-hand side of the Periodic Table (columns IA through VIB) which does *not* melt out of the bcc structure at ambient pressure. As we demonstrated in Ref. 6, the bcc structure is mechanically unstable at low pressure with a negative C' shear elastic constant for

atomic volumes $\Omega > 0.93\Omega_0$, where Ω_0 is the observed equilibrium volume. In this paper we show that, as a consequence, the hcp-bcc phase line ends in a triple point on the melting curve at about 4 GPa. Above that pressure, magnesium behaves more similarly to other simple metals with a close-packed low-temperature phase and a high-temperature bcc phase stabilized by soft T_1 [110] phonons.

Our primary statistical mechanics tools for treating magnesium at finite temperature are quasiharmonic lattice dynamics (QHLD), liquid variational perturbation theory[7–9] (VPT), and molecular-dynamics (MD) simulation. In Ref. 6 we showed that the quasiharmonic approximation yields an accurate description of most properties of the high-temperature solid. In particular, anharmonic corrections to hcp and bcc free energies, as estimated from a standard cell model,[10] were shown to have a negligible impact on the hcp-bcc phase line even at 1000 K. In this paper, the smallness of anharmonic effects is confirmed through direct molecular-dynamics simulation, and we use quasiharmonic lattice dynamics both to extend the hcp-bcc phase line to higher temperature and to provide solid free energies for melting. We then employ variational perturbation theory based on an r^{-12} reference system[8] to calculate corresponding liquid free energies, so that a complete temperature-pressure phase diagram can be calculated. This procedure is here benchmarked by molecular dynamics through a detailed study of melting out of the bcc structure near 30 GPa.

In Sec. II, we first briefly discuss our first-principles GPT potentials for magnesium and the calculation of thermodynamic functions using the baseline QHLD and VPT techniques. Then in Sec. III, we elaborate our MD simulations of melting and the benchmarking of our calculational procedure for obtaining the phase diagram. In Sec. IV, we present and discuss our calculated phase diagram together with computed melting properties near ambient pressure, which can be directly compared with experiment. We conclude in Sec. V.

II. FIRST-PRINCIPLES INTERATOMIC POTENTIALS AND THE CALCULATION OF THERMODYNAMIC FUNCTIONS

Below about 100 GPa in pressure, magnesium is a good nearly free-electron metal which is well described by the simple-metal limit of the GPT, as discussed in Ref. 6. In this limit a plane-wave basis is employed and the electron density and total energy are expanded in terms of weak nonlocal pseudopotential matrix elements. To second order in the pseudopotential, the real-space total-energy functional can be expressed as a large volume term plus a smaller pairwise sum over a two-ion central-force interatomic potential:

$$E_{\rm tot}(\mathbf{R}_1 \cdots \mathbf{R}_N) = N E_{\rm vol}(\Omega) + \frac{1}{2} \sum_{i,j}{}' v_2(R_{ij},\Omega) , \quad (1)$$

where Ω is the atomic volume, $R_{ij} \equiv |\mathbf{R}_i - \mathbf{R}_j|$ is the distance between ions i and j, and the prime on the summation excludes the $i=j$ term. The functions $E_{\rm vol}(\Omega)$ and $v_2(r,\Omega)$ both depend on the atomic volume Ω but are independent of structure and transferable to all bulk solid and liquid phases. In the simple-metal limit, the pair potential v_2 takes the form of a screened Coulomb potential given by

$$v_2(r,\Omega) = \frac{(Z^* e)^2}{r} \left[1 - \frac{2}{\pi} \int_0^\infty F_N(q,\Omega) \frac{\sin(qr)}{q} dq \right] , \quad (2)$$

where Z^* is an effective valence and F_N is a normalized energy-wave-number characteristic given by Eq. (3) of Ref. 6. These quantities are volume-dependent functionals of the atomic component of the pseudopotential. Both the volume term $E_{\rm vol}$ and the pair potential v_2 can be evaluated entirely from first principles with only the atomic number ($Z_a = 12$) and valence ($Z = 2$) as input. The calculated behavior of $v_2(r,\Omega)$ for magnesium at four equally spaced volumes is illustrated in Fig. 1. The general energy scale of these potentials is 10^{-3} Ry and that of structural-energy differences between solid phases, with the magnitude of the first minimum less than 2 mRy. Note that the position of this minimum is almost independent of volume but moves to positive energy under sufficient compression. As was discussed in Ref. 6, this behavior is consistent with the high-pressure hcp $\rightarrow$ bcc phase transition. In contrast, the long-range oscillations of $v_2(r,\Omega)$ are strongly volume dependent and asymptotically approach the familiar Friedel form [$v_2 \propto \sin(2k_F r)/r^3$]. In applying these potentials, we cut off the oscillatory tail of $v_2(r,\Omega)$ at $r = 8.25 R_{\rm WS}$ for each volume $\Omega = 4\pi R_{\rm WS}^3/3$, as was done in Ref. 6. Real-space sums centered on a given ion then typically include 525–550 nonzero near-neighbor interactions, which is sufficient to maintain both accurate and smoothly varying thermodynamic functions.

Free energies and other thermodynamics functions in metals can be partitioned into zero-temperature, ion-thermal, and electron-thermal contributions. Here the

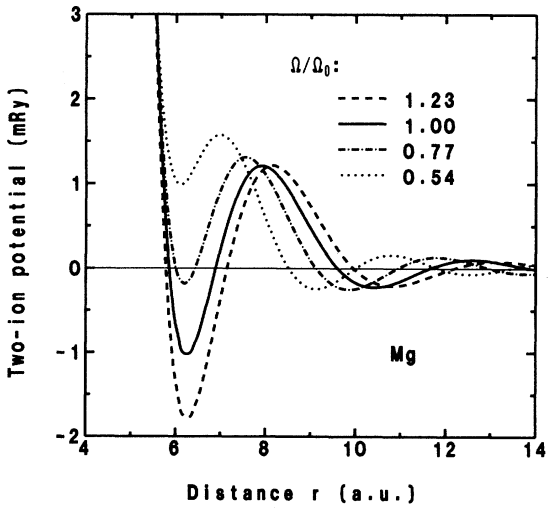

FIG. 1. First-principles GPT interatomic potentials for magnesium calculated at four equally spaced atomic volumes Ω. Here Ω_0 is the observed equilibrium volume of 156.8 a.u.

zero-temperature components of a given solid phase can be obtained directly from Eq. (1) evaluated for the appropriate crystal structure, while the ion-thermal components, arising from ion motion, must be provided by statistical mechanics. Electron-thermal components, on the other hand, arising from the excitation of electrons above the Fermi level E_F, are negligibly small in simple metals like magnesium at the temperatures of interest for the phase diagram. This is due both to the small, nearly free-electron density of electronic states at E_F and the fact that $k_B T_m \ll E_F$, where T_m is the melting temperature. Neglecting the electron-thermal contribution, the Helmholtz free energy per ion of any given solid phase, $A_{\rm sol}$, is then

$$A_{\rm sol}(\Omega,T)=E_0(\Omega)+A_{\rm ion}(\Omega,T)\ , \tag{3}$$

where $E_0=E_{\rm tot}/N$ and $A_{\rm ion}$ is the corresponding ion-thermal free energy. In general, $A_{\rm ion}$ will have both quasiharmonic and anharmonic contributions. In our baseline QHLD treatment, however, the latter is neglected entirely and the quasiharmonic contribution is calculated from the standard expression

$$A_{\rm ion}^{qh}(\Omega,T)=k_B T\sum_{\mathbf{q},\lambda}\ln\{2\sinh[h\nu_\lambda(\mathbf{q})/(2k_B T)]\}\ . \tag{4}$$

Here the phonon frequencies $\nu_\lambda(\mathbf{q})$ are implicit functions of volume and the sum is over all phonon wave vectors $\mathbf{q}$ and branches λ in the first Brillouin zone of the lattice. The required phonons in Eq. (4) can be calculated from standard lattice-dynamics theory in terms of tangential and radial force-constant functions, K_t and K_r, which, in turn, can be obtained analytically from Eq. (2):

$$K_t(r,\Omega)\equiv\frac{1}{r}\frac{\partial v_2(r,\Omega)}{\partial r}$$
$$=-\frac{(Z^*e)^2}{r^3}\left[1-\frac{2}{\pi}\int_0^\infty F_N(q,\Omega)\left[\frac{\sin(qr)}{q}-r\cos(qr)\right]dq\right] \tag{5}$$

and

$$K_r(r,\Omega)\equiv\frac{\partial^2 v_2(r,\Omega)}{\partial r^2}$$
$$=2\frac{(Z^*e)^2}{r^3}\left[1-\frac{2}{\pi}\int_0^\infty F_N(q,\Omega)\left[[1-(qr)^2/2]\frac{\sin(qr)}{q}-r\cos(qr)\right]dq\right]\ . \tag{6}$$

In this work, Eqs. (3) and (4) are applied to both the hcp and bcc phases of magnesium over a volume range $193.05<\Omega<69.80$ a.u. ($1.23<\Omega/\Omega_0<0.44$ with $\Omega_0=156.8$ a.u.) and a temperature range $0<T<3500$ K. As in Ref. 6, the c/a ratio for the hcp structure is fixed at 1.62, which approximately minimizes the hcp total energy at all volumes. The resulting minimum-energy hcp phase is found to be mechanically stable with real phonon frequencies over the entire volume range considered, while the bcc phase is stable only for volumes $\Omega<145.8$ a.u. ($\Omega/\Omega_0<0.93$). In evaluating the right-hand side of Eq. (4), we sample phonon frequencies at 252 and 1240 $\mathbf{q}$ points in the irreducible wedges of the hcp and bcc Brillouin zones, respectively.

As previous experience on aluminum and other simple metals[11,12] has shown, an appropriate complement of QHLD in the solid is VPT based on an r^{-12} reference system for the liquid. In VPT an upper bound on the liquid free energy per ion, $A_{\rm liq}$, is established by the rigorous Gibbs-Bogolyubov inequality:[7]

$$A_{\rm liq}(\Omega,T)\le A_{\rm liq}^{\rm max}(\Omega,T)\ , \tag{7}$$

where

$$A_{\rm liq}^{\rm max}(\Omega,T)=E_{\rm vol}(\Omega)+A_{\rm ref}(z)+(2\pi/\Omega)\int_0^\infty g_{\rm ref}(r,z)[v_2(r,\Omega)-v_{\rm ref}(r,z)]r^2dr\ . \tag{8}$$

Here $A_{\rm ref}$, $g_{\rm ref}$, and $v_{\rm ref}$ are the free energy, pair-correlation function, and pair potential of the reference system, where

$$v_{\rm ref}(r,z)=\epsilon(\sigma/r)^{12}\ , \tag{9}$$

$z=(\sigma^3/\sqrt{2}\Omega)(\epsilon/k_B T)^{1/4}$, and $A_{\rm ref}(z)$ and $g_{\rm ref}(r,z)$ are known functions.[8] At each volume and temperature of interest, the variational parameter z can be chosen to minimize the right-hand side of Eq. (8), so that in practice $A_{\rm liq}^{\rm max}$ becomes a very close upper bound to the true liquid free energy $A_{\rm liq}$. With the equal sign in Eq. (7) thereby approximately satisfied, Eq. (8) is then applied to obtain $A_{\rm liq}$ over the same volume range as in the solid and a temperature range $500<T<3500$ K. This is our baseline treatment of the liquid.

In calculating solid and liquid pressures from the above free energies, we have found it both convenient and useful to incorporate one minor *ad hoc* modification, which normalizes the pressure scale, into our otherwise first-principles procedure. As in any LDA calculational scheme, there is a small offset here between the calculated and the observed equilibrium atomic volume Ω_0. In magnesium with Eq. (1), Ω_0 is overestimated by 4.2 a.u. or 2.7%, which corresponds to an overestimate in pressure of 1.8 GPa at $T=300$ K. As we noted in Ref. 6, the

equation of state is approximately corrected by subtracting from it a pressure $\Delta P = 1.8$ GPa at all volumes and temperatures. Formally, this can be accomplished in a thermodynamically consistent manner by adding a term $\Delta P(\Omega - \Omega_0)$ to the volume term $E_{\rm vol}(\Omega)$, and in all applications of Eq. (1) below this has been done implicitly. At high pressure, of course, this modification is of little consequence. At low pressure, on the other hand, the normalized pressure scale allows one to make comparisons with experiment at the correct atomic volumes, which is important, for example, in analyzing melting properties.

III. MOLECULAR-DYNAMICS SIMULATIONS

To examine the adequacy of our baseline QHLD treatment of the solid and VPT treatment of the liquid, we have performed MD simulations on magnesium over a wide temperature range at a single compressed volume of $\Omega = 113.3$ a.u., where the bcc structure is mechanically stable and melting corresponds to a bcc $\rightarrow$ liquid phase transition. In these simulations we have treated 1024 ions in a constant-Ω, constant-T ensemble. Constant volume Ω is maintained by performing each simulation in a cubic box with periodic boundary conditions applied to the sides of the box. Constant temperature T is maintained with a Gaussian thermostat,[13-15] which is introduced through a friction term in modified Newtonian equations of motion for the ions:

$$\ddot{\mathbf{R}}_i = \mathbf{F}_i/m - \xi\dot{\mathbf{R}}_i \ , \tag{10}$$

where $\mathbf{F}_i$ the total force on ion i,

$$\mathbf{F}_i = -\sum_j{}' K_t(R_{ij},\Omega)\mathbf{R}_{ij} \ , \tag{11}$$

with K_t calculated from Eq. (5), and where the effective friction coefficient ξ is given by

$$\xi = \sum_j \dot{\mathbf{R}}_j\cdot(\mathbf{F}_j/m) \Big/ \sum_j \dot{\mathbf{R}}_j\cdot\dot{\mathbf{R}}_j \ . \tag{12}$$

Here the coupled equations of motion (10) are integrated with a standard velocity-Verlet algorithm[14] using a time step of approximately 1×10^{-15} sec (1 fsec).

The thermodynamic and structural properties of magnesium have thereby been explored in the temperature range $500 < T < 8000$ K. Beginning at 500 K in the bcc solid, we have moved upward in increments of $\Delta T = 500$ to 2500 K, where the increment has been reduced to 100 K through the melting transition. Once in the liquid, data has been accumulated from 2400 to 3000 K at $\Delta T = 300$ K, from 3000 to 4000 K at $\Delta T = 500$ K, and from 4000 to 8000 K at $\Delta T = 1000$ K. In each simulation, we begin with positions and scaled velocities for the ions from a previously equilibrated run at the closest nearby temperature. We then run 4000–8000 time steps to establish a good thermodynamic equilibrium and an additional 8000 time steps to gather statistics for the calculation of thermal energies and pressures, $E_{\rm ion}$ and $P_{\rm ion}$, and various structural properties such as the pair correlation function, $g(r)$. In the vicinity of melting, the number of latter time steps has been increased to 40 000 to make an accurate determination of the mechanical melting point. This is found to be 2650±50 K which corresponds to an average pressure of 31.3 GPa. Melting is indicated by sharp increases in $E_{\rm ion}$ and $P_{\rm ion}$ as well as by clear qualitative discontinuities in all structural properties. Figure 2 illustrates our calculated $g(r)$ for magnesium in the low-temperature bcc solid, near melting, and in

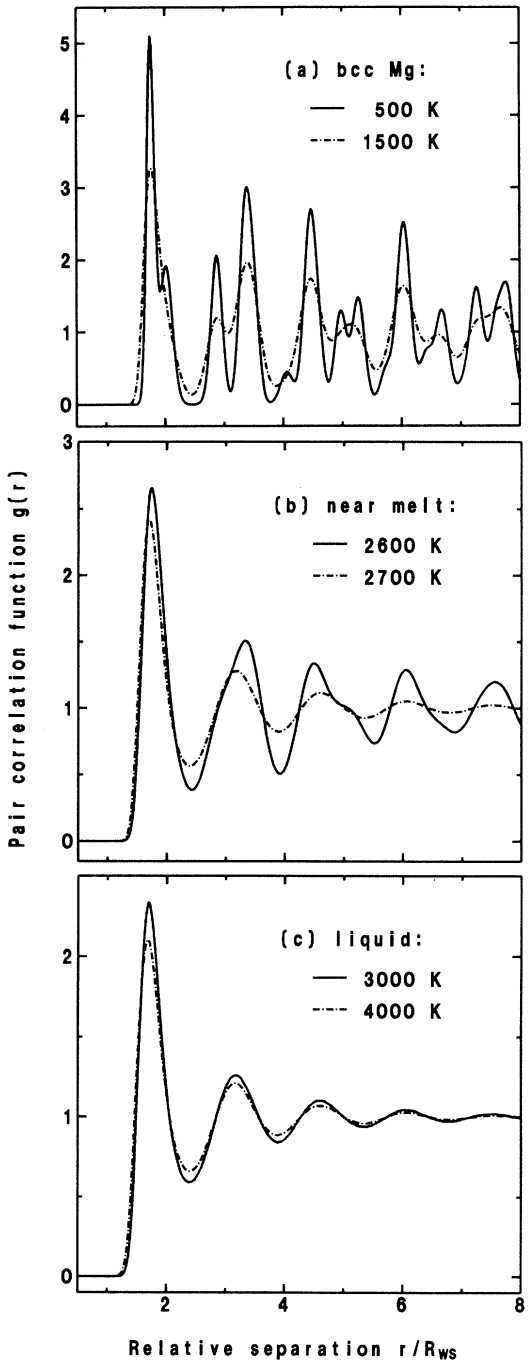

FIG. 2. Pair correlation function, $g(r)$, in solid and liquid magnesium at $\Omega = 113.3$ a.u., as determined from the present MD simulations: (a) in the bcc solid; (b) near melting; and (c) in liquid.

the high-temperature liquid. The loss of long-range order in $g(r)$ as one passes from 2600 to 2700 K is clearly evident in the figure.

The ion-thermal energy and pressure are calculated as:

$$E_{\rm ion}(\Omega,T)=\langle E_{\rm tot}\rangle/N-E_0(\Omega) \tag{13}$$

and

$$P_{\rm ion}(\Omega,T)=\langle -dE_{\rm tot}/d\Omega\rangle/N+dE_0(\Omega)/d\Omega\ , \tag{14}$$

respectively, where $\langle\cdots\rangle$ denotes a thermal average over the 1024-ion ensemble. Our MD results for these quantities in both the bcc solid and the liquid are plotted in Fig. 3. In the solid we find that $E_{\rm ion}$ and $P_{\rm ion}$ indeed remain very close to their high-temperature quasiharmonic limits of $3k_BT$ and $3k_BT\gamma/\Omega$, respectively, where γ is the Grüneisen parameter, which can be calculated directly from the bcc phonons:

$$\gamma(\Omega)=-(\Omega/3N)\sum_{\mathbf{q},\lambda}\frac{\partial\ln[h\nu_\lambda(\mathbf{q})]}{\partial\Omega}\ . \tag{15}$$

At $\Omega=113.3$ a.u., we obtain $\gamma=1.317$ from Eq. (15). The corresponding quasiharmonic value of the Debye temperature at this volume is calculated to be 509 K.

The thermal energies can also be used to obtain solid and liquid free energies and an estimate of the equilibrium thermodynamic melting point implied by our MD simulations. To do this we follow the general procedure developed in Ref. 16 for a similar study on the melting curve of molybdenum. We first note that the small anharmonic portion of the thermal energy in the bcc solid, $E_{\rm ion}^{\rm ah}$, can be extracted from the MD data as $E_{\rm ion}^{\rm ah}=E_{\rm ion}-3k_BT$ and fit to the polynomial form

$$E_{\rm ion}^{\rm ah}(\Omega,T)=-A_2T^2-2A_3T^3-3A_4T^4\ . \tag{16}$$

The expansion coefficients A_n, which in general are volume dependent, are determined by making a least-squares fit to the MD data. Equation (16) then can be readily integrated to yield the corresponding anharmonic component of the ion-thermal free energy:

$$\begin{aligned}A_{\rm ion}^{\rm ah}(\Omega,T)&=-T\int_0^T[E_{\rm ion}^{\rm ah}(\Omega,T')/(T')^2]dT'\\&=A_2T^2+A_3T^3+A_4T^4\ .\end{aligned} \tag{17}$$

The total solid free energy is obtained by simply adding this result to Eqs. (3) and (4):

$$\begin{aligned}A_{\rm sol}(\Omega,T)=&E_0(\Omega)\\&+k_BT\sum_{\mathbf{q},\lambda}\ln\{2\sinh[h\nu_\lambda(\mathbf{q})/(2k_BT)]\}\\&+A_2T^2+A_3T^3+A_4T^4\ .\end{aligned} \tag{18}$$

In the liquid phase, the entire ion-thermal free energy, $A_{\rm ion}^{\rm liq}$, can be obtained from the MD data, apart from an additive constant. Specifically, the first line of Eq. (17) is replaced by

$$\begin{aligned}&A_{\rm ion}^{\rm liq}(\Omega,T)/T\\&\quad=C_0(\Omega)/T_0-\int_{T_0}^T[E_{\rm ion}^{\rm liq}(\Omega,T')/(T')^2]dT'\ ,\end{aligned} \tag{19}$$

where T_0 is a reference temperature and $C_0(\Omega)\equiv A_{\rm ion}^{\rm liq}(\Omega,T_0)$. Allowing for an additional term linear in T, the temperature dependence of $E_{\rm ion}^{\rm liq}$ can be represented by a generalized expansion of the form

$$E_{\rm ion}^{\rm liq}(\Omega,T)=C_1\tau-C_2\tau^2-2C_3\tau^3-3C_4\tau^4\ , \tag{20}$$

where $\tau\equiv T/T_0$ and where the expansion coefficients C_1, C_2, C_3, and C_4 are again determined from a least-squares fit to the MD data. Using this result back in Eq. (19) and adding a zero-temperature contribution, one thus obtains

$$\begin{aligned}A_{\rm liq}(\Omega,T)=&E_0(\Omega)+C_0\tau-C_1\tau\ln\tau+C_2\tau(\tau-1)\\&+C_3\tau(\tau^2-1)+C_4\tau(\tau^3-1)\ .\end{aligned} \tag{21}$$

It then remains to determine the single constant C_0 in Eq. (21). This can be done very accurately using a technique developed by Boercker and Young[9] based on elements of VPT. In addition to the usual upper bound on $A_{\rm liq}$ established by Eqs. (7) and (8), a corresponding lower bound on the liquid free energy, $A_{\rm liq}^{\rm min}$, can be established by interchanging the roles of the true and the reference systems. This yields

$$A_{\rm liq}(\Omega,T)\geq A_{\rm liq}^{\rm min}(\Omega,T)\ , \tag{22}$$

where

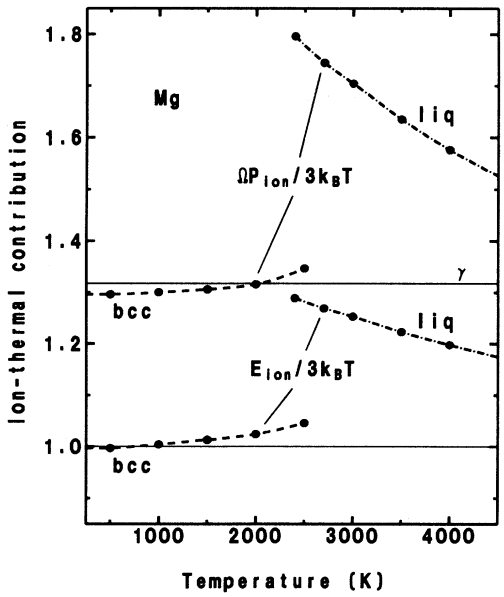

FIG. 3. Thermal energies and pressures, $E_{\rm ion}(\Omega,T)$ and $P_{\rm ion}(\Omega,T)$, in solid and liquid magnesium at $\Omega=113.3$ a.u., as determined from the present MD simulations. Here the solid points represent the actual MD data, while the dashed and dot-dashed lines are polynomial fits to the data. The reference line $\gamma=1.317$ is the quasiharmonic value of the Grüneisen parameter calculated from Eq. (15).

$$A_{\rm liq}^{\rm min}(\Omega,T)=E_{\rm vol}(\Omega)+A_{\rm ref}(z)+(2\pi/\Omega)\int_0^\infty g(r)[v_2(r,\Omega)-v_{\rm ref}(r,z)]r^2dr\ . \tag{23}$$

Here $g(r)$ is the true pair-correlation function for v_2 and in our case is directly determined from the MD simulations. The variational parameter z can now be chosen to maximize $A_{\rm liq}^{\rm min}$, making it a close lower bound to $A_{\rm liq}$. At high temperature the range between $A_{\rm liq}^{\rm min}$ and $A_{\rm liq}^{\rm max}$ becomes very narrow, so that an accurate value of $A_{\rm liq}$ can be calculated by taking the average

$$A_{\rm liq}(\Omega,T)=\tfrac{1}{2}[A_{\rm liq}^{\rm min}(\Omega,T)+A_{\rm liq}^{\rm max}(\Omega,T)]\ . \tag{24}$$

We have evaluated Eq. (24) at a reference temperature of $T_0=4000$ K and used the result in Eq. (21) to obtain $C_0=-0.19660$ Ry. We have verified that $A_{\rm liq}$ given by Eq. (21) is basically insensitive to where Eq. (24) is evaluated, by applying the latter at 8000 K and then integrating $E_{\rm ion}^{\rm liq}$ down to 4000 K via Eq. (19) to obtain $C_0=-0.19685$ Ry. The resulting small uncertainty of 0.25 mRy leads to an uncertainty of about 30 K in the melting temperature.

To finally calculate a thermodynamic melting point from our MD data at a single atomic volume Ω, we follow a well-established procedure[17] which accurately approximates the rigorous common-tangent construction between $A_{\rm sol}$ and $A_{\rm liq}$. Specifically, we interpret Ω as the average volume of melting and equate free energies from Eqs. (18) and (21) to obtain a melting temperature T_m:

$$A_{\rm sol}(\Omega,T_m)=A_{\rm liq}(\Omega,T_m)\ . \tag{25}$$

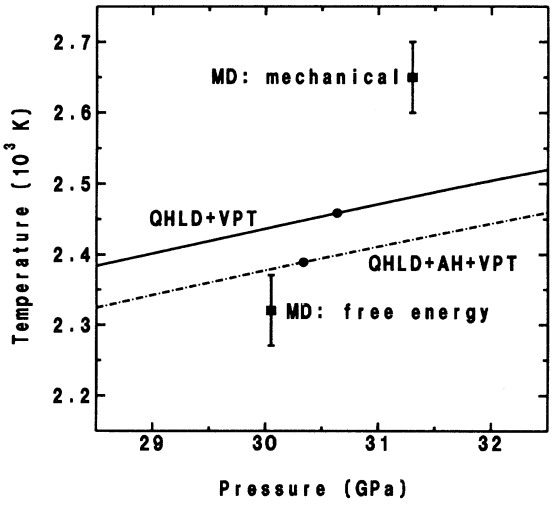

FIG. 4. Calculated melting temperatures of magnesium near 30 GPa, as obtained from the present MD simulation studies (solid square points) and the baseline QHLD plus VPT treatment (solid line and accompanying solid circular point) discussed in the text. The dot-dashed line result adds an anharmonic cell-model contribution to the baseline treatment. The solid and dot-dashed lines have been derived from common-tangent constructions between solid and liquid free energies, while the lower three solid points have been calculated from Eqs. (25) and (26) using data at a single atomic volume ($\Omega=113.3$ a.u.).

The corresponding melting pressure is then calculated as the average

$$P_m=\tfrac{1}{2}[P_{\rm sol}(\Omega,T_m)+P_{\rm liq}(\Omega,T_m)]\ . \tag{26}$$

We thereby obtain $T_m=2320$ K at $P_m=30.0$ GPa, which is about 15% lower in temperature than the mechanical melting point observed in our MD simulations. The difference can be attributed to the usual superheating of the solid prior to melting occurring in direct mechanical simulations. These MD values of T_m are compared with the melting curve obtained from our baseline QHLD plus VPT treatment in Fig. 4. The latter is based on a full common-tangent construction, using Eqs. (3) and (4) for the solid free energy and Eqs. (7) and (8) for the liquid free energy, but we have also verified the accuracy of Eqs. (25) and (26) in this context, as shown in Fig. 4. The QHLD + VPT curve in this figure is seen to lie about 100 K or 4% above the MD free-energy point. We regard this as a quite tolerable error, especially considering the enormous computational simplification that our baseline treatment provides. We have further noted that if an anharmonic cell-model[10] contribution is included in the solid free energy, this error is approximately halved, as also shown in Fig. 4. Closer inspection, however, indicates that the latter improvement is somewhat fortuitous. In fact, anharmonic effects here are sufficiently small and subtle that, other than their general magnitude, the cell model does not appear to describe them accurately. For this reason, we prefer the QHLD plus VPT treatment.

IV. PHASE DIAGRAM AND MELTING PROPERTIES

Using the baseline solid and liquid free energies discussed above, the full phase diagram of magnesium has been calculated to 3500 K in temperature and 60 GPa in pressure. This result is plotted in Fig. 5 and compared with existing experimental data on the hcp-bcc phase boundary near 50 GPa from room-temperature diamond-anvil-cell measurements[4] and on the melting curve below 4 GPa from early piston-cylinder measurements.[18] The agreement is seen to be very good in both cases. The qualitative features of the calculated phase diagram are similar to those of the earlier semiempirical result of Pélissier,[19] but quantitatively, the present phase diagram appears to be considerably more accurate. The highly temperature dependent hcp-bcc phase line is here predicted to end in a triple point on the melting curve at 1180 K and 4.3 GPa. The unusual dip in the hcp-bcc line near the triple point is an artifact of the extreme softness of T_1 [110] bcc phonons in this region and is a real prediction of the theory. Below 4.3 GPa, the bcc structure becomes mechanically unstable with the long-wavelength T_1 [110] phonon modes calculated to be imaginary. This behavior explains the well-known absence of a high-temperature bcc phase in magnesium at ambient pressure. It is also interesting to note that the rapid tempera-

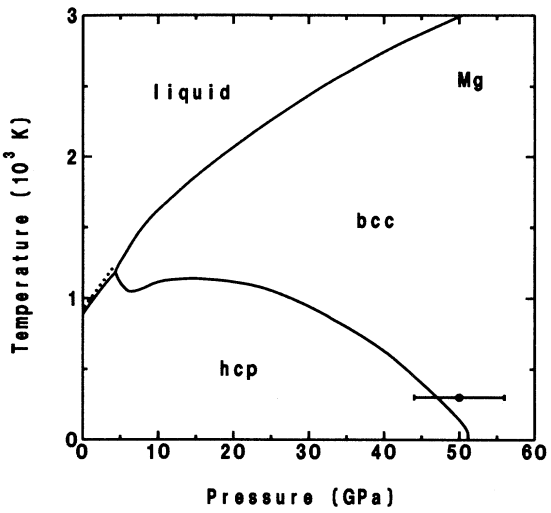

FIG. 5. Temperature-pressure phase diagram of magnesium, as obtained from the baseline QHLD plus VPT approach discussed in the text (solid lines). The solid point with error bars represents the diamond-anvil-cell measurements of Ref. 4 for the hcp → bcc transition, while the dots represent the experimental melting curve of Ref. 18.

TABLE I. Melting properties of magnesium at zero pressure, as calculated from the baseline QHLD plus VPT approach and compared with experiment. Quantities and units: melting temperature T_m in K; solid and liquid volumes Ω_{sol} and Ω_{liq} in a.u.; $\Delta\Omega=\Omega_{liq}-\Omega_{sol}$; latent heat L in mRy/atom; entropy change ΔS in k_B; melting-curve slope dT_m/dP_m in K/kbar; liquid specific heat c_p^{liq} in k_B; and liquid sound speed v_s^{liq} in km/sec.

Quantity	Present theory	Experiment
T_m	885	922[a]
Ω_{sol}	165.6	163.3[b]
Ω_{liq}	175.1	171.3[c]
$\Delta\Omega$	9.5	8.0[b]
L	7.16	6.82[a]
$\Delta S/k_B$	1.28	1.17[a]
dT_m/dP_m	8.0	7.4[d]
c_p^{liq}/k_B	3.8	3.9[a]
v_s^{liq}	4.34	4.065[e]

[a]Reference 20.
[b]Inferred from Eq. (30) using the measured values of dT_m/dP_m, T_m, L, and Ω_{liq}.
[c]Reference 21.
[d]Reference 18.
[e]Reference 22.

ture dependence of the hcp-bcc phase line implies that there is a corresponding rapid tradeoff between the two different physical mechanisms which stabilize the bcc structure above this line at high and low temperature. At low pressure and high temperature, the dominant stabilizing mechanism is the large entropy contribution to the free energy produced by the soft bcc phonons. At high pressure and low temperature, on the other hand, phonons play no important role and the bcc structure is instead stabilized by subtle electronic-structure effects connected with $sp \rightarrow d$ electron transfer.[3] These latter effects are embodied directly in the short-range part of the interatomic potentials.[3,6]

Calculated melting properties at zero pressure are given in Table I and compared with available experimental data.[18,20–22] Included are the melting temperature T_m; solid and liquid volumes, Ω_{sol} and Ω_{liq}, and the corresponding volume change

$$\Delta\Omega \equiv \Omega_{liq} - \Omega_{sol} \ ; \tag{27}$$

the latent heat L and the corresponding entropy change

$$\Delta S = L/T_m \ ; \tag{28}$$

the initial slope of the melting curve, dT_m/dP_m; the constant-pressure specific heat in the liquid, c_p^{liq}; and the liquid sound speed

$$v_s^{liq} = (B_s^{liq}/\rho_{liq})^{1/2} \ , \tag{29}$$

where B_s^{liq} and ρ_{liq} are the adiabatic bulk modulus and the density, respectively, in the liquid. The experimental values listed are directly measured quantities except for Ω_{sol} and $\Delta\Omega$, which have been inferred from the Clausius-Clapeyron relation

$$dT_m/dP_m = T_m \Delta\Omega/L \ , \tag{30}$$

and for ΔS, which has been inferred from Eq. (28). The agreement between theory and experiment is within 10% for all quantities considered except $\Delta\Omega$, which is overestimated by about 19%.

V. CONCLUSIONS

In this work we have successfully combined first-principles GPT interatomic potentials with quasiharmonic lattice dynamics in the solid and with variational perturbation theory in the liquid to calculate a complete and accurate temperature-pressure phase diagram for magnesium. The validity of the latter statistical mechanics tools for this application has been directly verified through molecular-dynamics simulations. These simulations confirm the smallness of anharmonic effects in the bcc solid and demonstrate that the bcc-liquid melting curve so obtained is accurate to about 4% for the given potentials. The hcp-liquid portion of the melting curve to 4 GPa and the hcp-bcc phase boundary near 50 GPa and 300 K are in good agreement with existing experimental data, as are calculated melting properties at zero pressure. The bcc-liquid portion of the melting curve, the high-temperature portion of the hcp-bcc phase line, and the hcp-bcc-liquid triple point near 1200 K and 4 GPa are predictions which await experimental investigation. These features of the phase diagram should all be experimentally accessible through the laser-heated diamond-anvil cell.

The success of our baseline QHLD plus VPT approach in magnesium also confirms our earlier successful applications[11,12] of this type of approach to the equation of state and high-pressure melting curves of aluminum and other metals which are well described by first-principles GPT

pair potentials. In none of the latter cases, however, has the full temperature-pressure phase diagram been investigated, although this would be of considerable interest. In aluminum, for example, a rapid sequence of high-pressure phase transitions, fcc → hcp → bcc, has been predicted above 100 GPa at zero temperature,[3] and one can expect a correspondingly rich phase diagram at high temperature. We hope to investigate this and other interesting cases in the future.

ACKNOWLEDGMENTS

Work supported by the U. S. Department of Energy: at Lawrence Livemore National Laboratory under Contract No. W-7405-Eng-48; at Sandia National Laboratories by the Office of Basic Energy Sciences, Division of Materials Science through a New Initiative under Contract No. DE-AC04-94AL8500.

[1]W. Kohn and L. J. Sham, Phys. Rev. **140**, A1133 (1965).
[2]For example, H. L. Skriver, Phys. Rev. B **31**, 1909 (1985).
[3]J. A. Moriarty and A. K. McMahan, Phys. Rev. Lett. **48**, 809 (1982); A. K. McMahan and J. A. Moriarty, Phys. Rev. B **27**, 3235 (1983).
[4]H. Olijnyk and W. B. Holzapfel, Phys. Rev. B **31**, 4682 (1986).
[5]J. A. Moriarty, Phys. Rev. B **16**, 2537 (1977); **26**, 1754 (1982); **38**, 3199 (1988).
[6]J. D. Althoff, P. B. Allen, R. M. Wentzcovitch, and J. A. Moriarty, Phys. Rev. B **48**, 13 253 (1993).
[7]N. W. Ashcroft and D. Stroud, in *Solid State Physics,* edited by F. Seitz, D. Turnbull, and H. Ehrenreich (Academic, New York, 1978), Vol. 33, p. 1, and references therein.
[8]D. A. Young and F. J. Rogers, J. Chem. Phys. **81**, 2789 (1984).
[9]D. B. Boercker and D. A. Young, Phys. Rev. A **40**, 6379 (1989).
[10]D. A. Young and M. Ross, J. Chem. Phys. **74**, 6950 (1981).
[11]J. A. Moriarty, D. A. Young, and M. Ross, Phys. Rev. B **30**, 578 (1984).
[12]W. J. Nellis, J. A. Moriarty, A. C. Mitchell, M. Ross, R. G. Dandrea, N.W. Ashcroft, N. C. Holmes, and G. R. Gathers, Phys. Rev. Lett. **60**, 1414 (1988), and references therein.
[13]W. G. Hoover, A. J. C. Ladd, and B. Moran, Phys. Rev. Lett. **48**, 1818 (1982); D. J. Evans, J. Chem. Phys. **78**, 3297 (1983).
[14]M. P. Allen and D. J. Tildesley, *Computer Simulation of Liquids* (Oxford University Press, Oxford, 1989).
[15]W. G. Hoover, *Computational Statistical Mechanics* (Elsevier, Amsterdam, 1991).
[16]J. A. Moriarty, Phys. Rev. B **49**, 12 431 (1994).
[17]J. A. Moriarty, Phys. Rev. B **8**, 1338 (1973).
[18]G. C. Kennedy and R. C. Newton, in *Solids Under Pressure,* edited by W. Paul and D. M. Warschauer (McGraw-Hill, New York, 1963), p. 163.
[19]J. L. Pélissier, Phys. Scr. **34**, 838 (1986).
[20]R. Hultgren, P. D. Desai, D. T. Hawkins, M. Gleiser, K. K. Kelly, and D. D. Wagman, *Selected Values of the Thermodynamic Properties of the Elements* (American Society for Metals, Metals Park, Ohio, 1973), p. 294.
[21]M. Shimoji, *Liquid Metals* (Academic, New York, 1977), p. 381.
[22]S. Blairs and U. Joasoo, J. Inorg. Nucl. Chem. **42**, 1555 (1980).